Supporting Information

Overby et al. 10.1073/pnas.1410602111

SI Text

Schlemm's Canal Monolayer Perfusions and Pore Counting. *Detailed methods.* Schlemm's canal (SC) cells were seeded at confluence and cultured for 2 d in serum-containing culture medium on the external bottom-facing surface of a polystyrene filter membrane insert (Corning Transwell 3470; 0.4-μm-diameter track-etched pores), following previously described methods (1). The filter membrane insert was sealed with a conical silicone stopper (Versilic; VWR) and the cells were perfused with serum-free medium at 37 °C in a basal-to-apical direction at 0 (control), 2 or 6 mmHg. After 30 min, the cells were immersed in fixative [2.5% (vol/vol) glutaraldehyde and 2.0% (wt/vol) paraformaldehyde in PBS; TAAB Laboratories Equipment] while perfusion with serum-free medium continued for an additional 30 min. The perfusion was then stopped, and the membrane insert was disconnected from the perfusion system and immersed in fixative for an additional 30 min. Standard procedures for scanning electron microscopy were used to examine the pores on a JSM 6390 scanning electron microscope (JEOL). To determine whether pore formation depended on the direction of perfusion, one SC cell strain (SC67) was perfused in the reverse apical-to-basal direction. For these experiments, SC cells were seeded on the internal top-facing surface of the filter membrane, such that flow crossed the cell layer in the apical-to-basal direction when the filter membrane insert was interfaced with the perfusion system.

Pore area and density (number of pores per square millimeter) were quantified by sampling 12 randomly selected regions for each cell layer. Each region (~5,500 μm^2) was imaged at 1,500× magnification using scanning electron microscopy and any pore-like feature was reimaged at 10,000× magnification. Pore counting was done in a masked fashion. Pores were defined as circular or elliptical openings through the cell layer with smooth edges (2, 3). Pores were characterized as transcellular (passing through an individual cell) or paracellular (intersecting the junction between two neighboring cells) as previously described (3).

Pore density. Transcellular and paracellular pore density increased with perfusion pressure for all three nonglaucomatous cell strains at 2 or 6 mmHg compared with unperfused controls at 0 mmHg ($P < 0.005$; Fig. S1 *A* and *B*). When the pressure drop was reversed to perfuse one cell strain (SC67) in the apical-to-basal direction at 6 mmHg, the paracellular pore density significantly decreased compared with basal-to-apical perfusion ($P < 10^{-6}$), whereas the decrease in transcellular pore density was not statistically significant. The increased subcortical stiffness in glaucomatous cell strains was significantly correlated with decreasing transcellular pore density ($P < 0.02$; Fig S1*C*), with a borderline significant correlation with decreasing paracellular pore density ($P < 0.07$; Fig S1*D*).

Pore area. The porosity (total pore area per unit cell area) increased significantly with perfusion pressure for all three normal cell strains when perfused in the basal-to-apical direction at 2 ($P < 0.019$) or 6 mmHg ($P < 0.004$) but not in the apical-to-basal direction at 6 mmHg ($P = 0.79$; SC67) relative to unperfused controls (Fig. S2*A*). In the three glaucomatous cell strains, porosity was markedly reduced compared with the three normal cell strains when perfused at 6 mmHg in the basal-to-apical direction ($P < 0.035$; Fig. S2*B*). The porosity seen in glaucomatous SC cell strains perfused at 6 mmHg was comparable to that of unperfused normal controls (Fig. S2 *A* and *B*).

For those two normal and three glaucomatous SC cell strains in which both cell stiffness and pore area were measured, increasing subcortical stiffness [measured by atomic force microscopy (AFM), 10-μm spherical tip] correlated with decreasing porosity ($P < 0.012$; Fig. S2*C*).

AFM Studies. ***Control studies.*** The AFM data as measured with both sharp and rounded tips were found to be non-Gaussian as determined using Q-Q plots (4) (Fig. S3 *A* and *B*). However, a log transformation of the data yielded a Gaussian distribution (Fig. S3 *C* and *D*) and thus the statistics used on the AFM data were done on log-transformed data.

Table S1 gives the *P* values (paired *t* test) for each tip geometry when comparing the mean values at the nuclear versus nonnuclear region for six normal and five glaucomatous strains. We concluded that there were no significant differences between AFM measurements in the nuclear and nonnuclear regions, similar to a conclusion we had drawn earlier on other endothelial cell types (5).

We investigated the possibility of a relationship between donor age and modulus as measured by AFM using the Pearson correlation coefficient. No such relationship was found (Table S2). Thus, even though the glaucomatous cell strains come from somewhat older individuals than do the normal cell strains, it is not likely that this can explain the difference between the AFM stiffnesses of normal and glaucomatous cells strains reported in this study.

Effect of latrunculin-A. To examine the contribution of the actin cytoskeleton to SC cell stiffness, normal and glaucomatous SC cells were treated with the actin-depolymerizing agent latrunculin-A, and then the cell stiffness was measured with AFM using sharp tips and larger rounded tips. Treatment led to complete depolymerization of the SC cell cortex and a very substantial reduction in stress fibers and fibrillar collagen (Fig. 3*A*); there was no apparent difference in filamentous actin distribution between normal and glaucomatous SC cells. Latrunculin-A caused a significant decrease in cell stiffness of both cortical and subcortical cytoskeleton in both normal and glaucomatous SC cells (Fig. S4), confirming the importance of actin to cell stiffness at both of these sites. There was no apparent difference in the relative decrease in cell stiffness caused by latrunculin-A when comparing normal to glaucomatous cells.

Optical Magnetic Twisting Cytometry Studies. ***Effect of cell passaging.*** We have previously evaluated the effect of cell passaging on the mechanical phenotype of SC cells (6). Cell stiffness, contractile response to FBS, and relaxing response to isoproterenol were relatively stable from passages 2–6.

AFM characterization of gels. A commercial AFM (MFP-3D; Asylum) was used with probes constructed with borosilicate spherical tips, nominal diameter 5 μm, glued to triangular Au-coated silicon nitride cantilevers with a nominal spring constant of 0.06 N/m (Novascan Technologies). Ten force-displacement curves were collected from each sample and used to determine gel modulus as a function of cross-linker concentration (Fig. S5). Maximum forces were set to ~1.5 nN.

Baseline studies. When SC cells were grown on a rigid substrate, we did not find any difference in their baseline cytoskeletal stiffness as measured using optical magnetic twisting cytometry (OMTC) between normal and glaucomatous SC cells (Fig. S6).

Effects of drugs that alter outflow resistance. We previously reported how normal SC cells respond differently to drugs with known effects on outflow resistance (6). Here we extend those results to glaucomatous SC cells. Sphingosine-1-phosphate (S1P), thrombin, and lysophosphatidic acid (LPA), all known to increase outflow resistance at the tissue level, promptly increased cell stiffness by up to 200% (Fig. S7). Conversely, latrunculin-A, isoproterenol, dibutryl cyclic-AMP (DBcAMP), or Y-27632, all known to decrease outflow resistance at the tissue level, dose-dependently decreased cell stiffness by up to 80% (Figs. S7 and S8). In the case of isoproterenol treatment, the lack of cytoskeletal softening correlated with the lack of β2 adrenergic receptor expression (Fig. S8*G*), consistent with our previous finding on normal SC cells alone (6). These results also extended another previous finding—that drugs that modulate outflow resistance also modulate SC cell stiffness in tandem (6)—from normal to glaucomatous cells (i.e., glaucoma SC cells are also responsive to treatments known to affect outflow resistance).

Statistical methods for gene expression studies. The effect of cell strain donor age was examined by adding this as an extra covariate to the regression analysis:

$$\frac{Variable(E_{Substrate})}{Variable(1.1\ \text{kPa})} - 1 = b_1 * \left(\frac{E_{Substrate}}{1.1\ \text{kPa}} - 1\right) + b_2 * \left(\frac{E_{Substrate}}{1.1\ \text{kPa}} - 1\right) * Normal + b_3 * \left(\frac{E_{Substrate}}{1.1\ \text{kPa}} - 1\right) * Age.$$

Only for three genes did this have any effect on the conclusions from the regression analysis. *MMP2* expression was found to decrease significantly with cell strain donor age ($P < 0.001$), to increase with substrate stiffness ($P < 10^{-4}$), and not to be affected by glaucoma ($P > 0.5$). *PAI1* was also found to decrease significantly with cell strain donor age ($P < 0.005$), to increase with substrate stiffness ($P < 0.02$), and not to be affected by glaucoma ($P > 0.5$). The marginally significant negative association with substrate stiffness in glaucomatous cells for PTGS2 was not distinguishable from a marginally significant negative association with aging.

Real-Time Quantitative PCR. The sequences of primers used are shown in Table S3.

1. Pedrigi RM, Simon D, Reed A, Stamer WD, Overby DR (2011) A model of giant vacuole dynamics in human Schlemm's canal endothelial cells. *Exp Eye Res* 92(1):57–66.
2. Sit AJ, Coloma FM, Ethier CR, Johnson M (1997) Factors affecting the pores of the inner wall endothelium of Schlemm's canal. *Invest Ophthalmol Vis Sci* 38(8): 1517–1525.
3. Ethier CR, Coloma FM, Sit AJ, Johnson M (1998) Two pore types in the inner-wall endothelium of Schlemm's canal. *Invest Ophthalmol Vis Sci* 39(11):2041–2048.
4. Moore D, McCabe G, Craig B (2009) *Introduction to the Practice of Statistics* (Freeman, New York), 6th Ed, pp 417–486.
5. Vargas-Pinto R, Gong H, Vahabikashi A, Johnson M (2013) The effect of the endothelial cell cortex on atomic force microscopy measurements. *Biophys J* 105(2):300–309.
6. Zhou EH, et al. (2012) Mechanical responsiveness of the endothelial cell of Schlemm's canal: Scope, variability and its potential role in controlling aqueous humour outflow. *J R Soc Interface* 9(71):1144–1155.

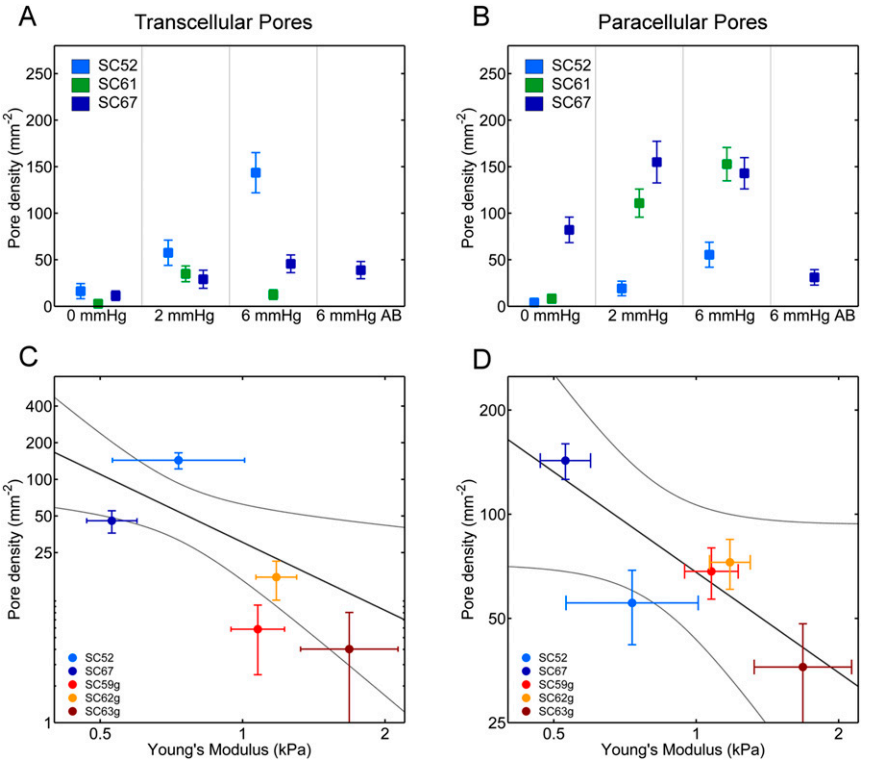

Fig. S1. Effects of pressure drop and subcortical stiffness on transcellular and paracellular pore density (number of pores per unit cell area). (*A*) Transcellular pore density increases in nonglaucomatous SC cell strains when perfused in the basal-to-apical direction at 2 or 6 mmHg ($P < 0.002$) relative to unperfused controls at 0 mmHg. (*B*) Paracellular pore density increases at 2 or 6 mmHg ($P < 0.005$) relative to 0 mmHg unperfused controls. Reversing the pressure drop in one SC cell strain (SC67) decreased the paracellular ($P < 10^{-6}$), but not transcellular, pore density. (*C*) There is a significant correlation (dark line) between decreasing transcellular pore density and increasing subcortical Young's modulus measured by AFM with 10-μm spherical tips ($P < 0.02$). (*D*) There is a borderline significant correlation (dark line) between decreasing paracellular pore density and increasing subcortical Young's modulus ($P < 0.07$). Bars represent SEM on pore density and modulus. Light curves in *C* and *D* represent 95% confident intervals on the slope of the generalized linear model (GLM) linear regression.

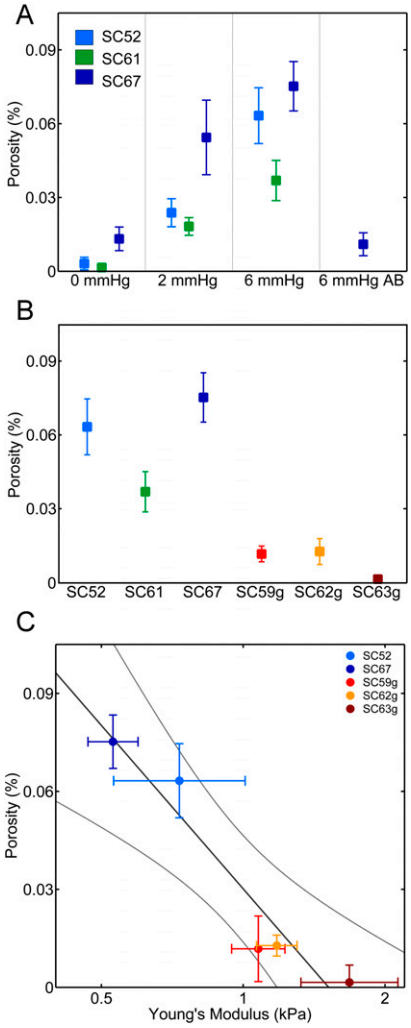

Fig. S2. Effects of pressure and glaucoma on porosity (pore area per unit cell area). (*A*) Porosity increases in three nonglaucomatous SC cell strains as a function of pressure drop in the basal-to-apical direction at 0, 2, or 6 mmHg. In the one SC cell strain (SC67) perfused in the apical-to-basal direction (AB) at 6 mmHg, porosity is similar to the unperfused controls at 0 mmHg. (*B*) Porosity is less in glaucomatous (SC59g, SC62g, and SC63g) compared with normal SC cells (SC52, SC 61, and SC67) following perfusion at 6 mmHg in the basal-to-apical direction. (*C*) There is a significant correlation (dark curve) between decreasing porosity and increasing Young's modulus as measured by AFM with 10-μm spherical tips. Bars represent SEM on porosity and modulus. Light curves in *C* represent 95% confident intervals on the slope of the GLM linear regression.

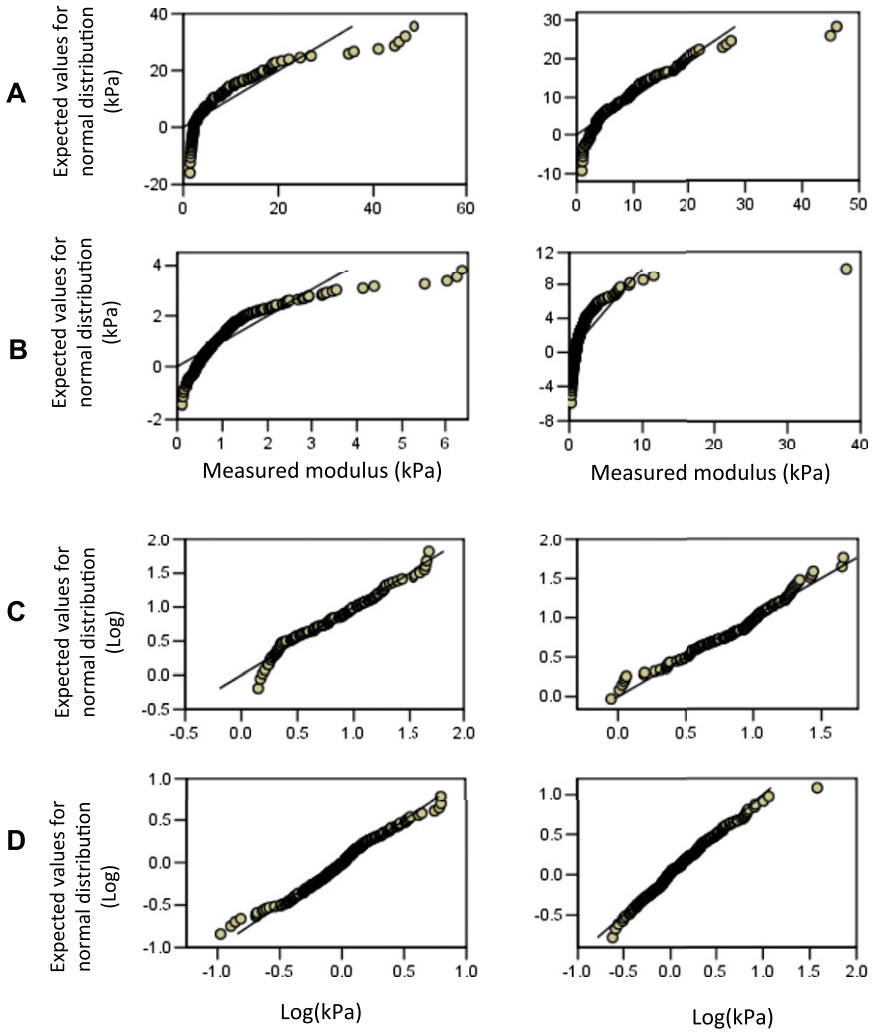

Fig. S3. Q-Q plots for AFM data. Plots compare the quantiles for the Young's modulus measured to the expected values if data follow a normal distribution. Left panels are for normal SC cells (SC41, SC51, SC52, SC58, SC60, and SC67); right panels are for glaucomatous SC cells (SC57, SC59, SC62, SC63, and SC64). (*A*) AFM modulus measurements using sharp tips. (*B*) AFM data measurements with 4.5- and 10-μm spherical tips. (*C*) AFM measurements with sharp tips after logarithmic transformation. (*D*) AFM data measurements with spherical tips after logarithmic transformation. All datasets follow a Gaussian distribution after the transformation.

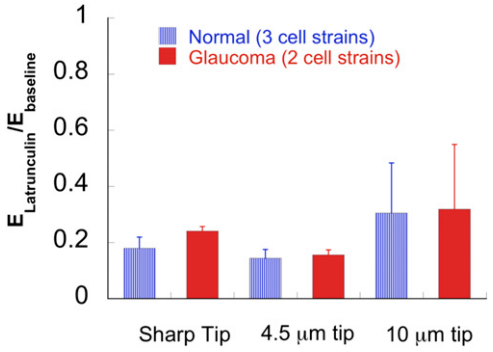

Fig. S4. Decrease in cell stiffness following latrunculin-A as measured by AFM. The ratio of the cell modulus measured after 30 min of treatment with latrunculin-A (1 μM) ($E_{latrunculin}$) compared with the cell modulus measured immediately before treatment with latrunculin ($E_{baseline}$) in the same population of cells. Measurements performed in two normal and three glaucomatous cell strains.

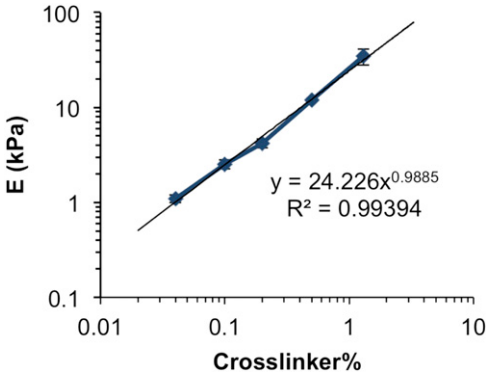

Fig. S5. Effect of cross-linker concentration on the stiffness of gels, measured using AFM. Mean ± SEM, $n = 10$ per data point.

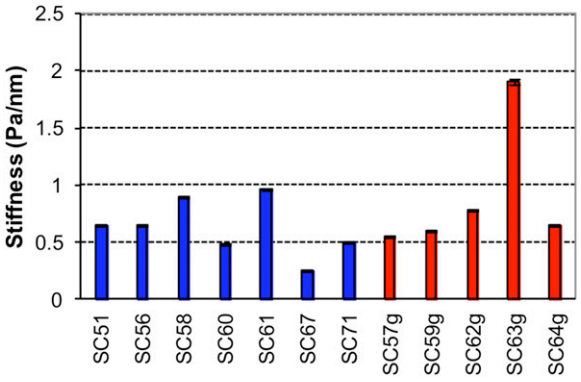

Fig. S6. Comparison of cell stiffness as measured by OMTC between normal and glaucomatous SC cells grown on rigid substrates. Cell stiffness (g) was measured using OMTC with cells grown on collagen-coated plastic as described previously (6). Median ± SEM with $n > 3{,}746$ beads for each donor; $P = 0.3$ by t test between normal ($n = 7$) and glaucoma strains ($n = 5$). Data for SC51, SC56, SC58, SC60, and SC61 were from our previous work (6) and are included here for comparison.

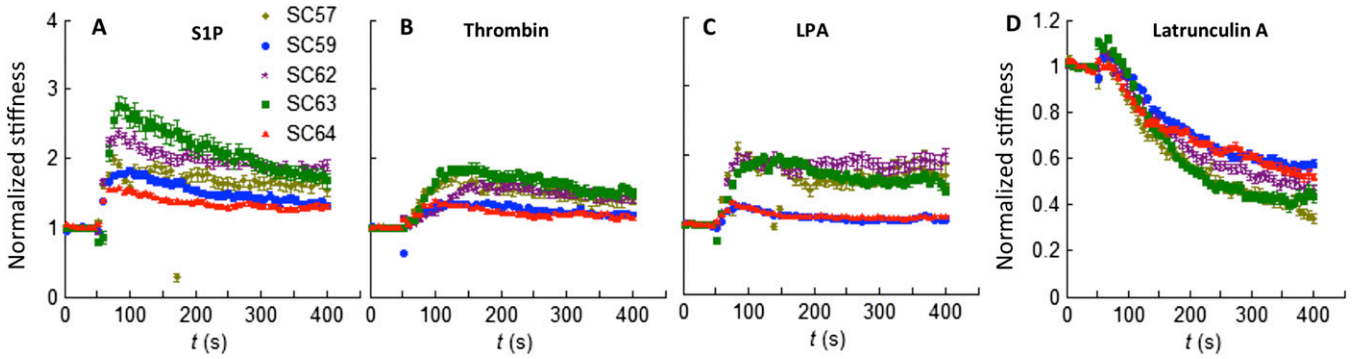

Fig. S7. The evolution of cell stiffness with time was monitored using OMTC while the indicated drug was introduced at ~50 s, as described previously (6). Similar to normal SC cells (6), glaucomatous SC cells contracted in response to S1P (*A*), thrombin (*B*), and LPA (*C*) and relaxed in response to latrunculin-A (*D*). Cell stiffness was normalized by predrug control. Median ± SEM with $n > 300$ beads for each data series. When we compared drug response at 300 s, there was no difference between normal ($n = 5$) (6) and glaucoma ($n = 5$); $P > 0.43$.

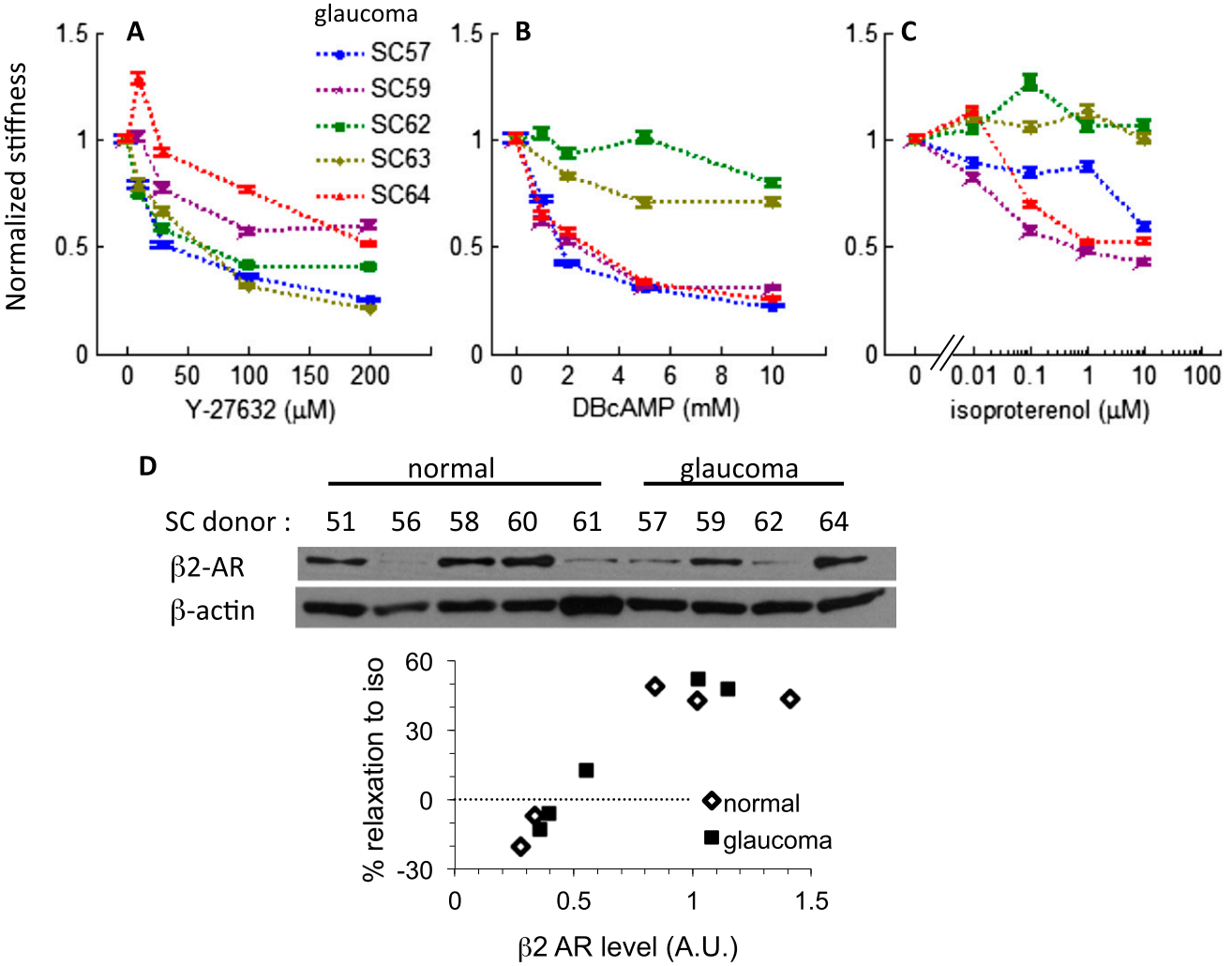

Fig. S8. The dose-dependent relaxation of SC cells was quantified using OMTC after ~45-min incubation with the indicated drug, as described previously (6). Similar to normal SC cells (6), glaucomatous cells also dose-dependently relaxed in response to Y-27632 (*A*), DBcAMP (*B*), and isoproterenol (*C*) in a donor-dependent manner. Median ± SEM with $n > 1{,}000$ beads for each data point. When we compared drug response at each dose for each drug, there was no difference between normal ($n = 5$) (6) and glaucoma ($n = 5$); $P > 0.26$. (*D*) The protein level of β2 adrenergic receptor was quantified using Western blot (*Upper*); the protein of SC63 was run on another blot and not shown. Protein level was positively correlated with the relaxation response to 1 μM isoproterenol (*Lower*). Data for normal SC cells were from our previous work (6) and are included here for comparison.

Table S1. Nucleus versus nonnuclear AFM measurements

AFM tip	*P* value for normal lines ($n = 6$)	*P* value for glaucomatous lines ($n = 5$)
Sharp	0.655 (m = 104)	0.071 (m = 148)
4.5-μm sphere	0.212 (m = 104)	0.928 (m = 122)
10-μm sphere	0.101 (m = 153)	0.735 (m = 111)

Paired *t* test, nucleus vs. cytoplasm. m, number of measurements.

Table S2. Correlation coefficient (r) of AFM measurement with donor age

AFM tip and cell strains	r	*P* value
4.5-μm sphere, all strains	−0.02	0.960
Normals (*n* = 6, m = 104)	−0.56	0.247
Glaucomas (*n* = 5, m = 128)	−0.19	0.759
10-μm sphere, all strains	0.33	0.329
Normals (*n* = 6, m = 153)	−0.28	0.590
Glaucomas (*n* = 5, m =120)	0.50	0.396
Sharp tip, all strains	0.39	0.235
Normals (*n* = 6, m = 104)	0.29	0.577
Glaucomas (*n* = 5, m = 148)	0.65	0.236

m, number of measurements; *n*, number of cells.

Table S3. Sequences of primers used for real-time RT-PCR

Gene	Sequence	Position
GAPDH	5′-AGCCACATCGCTCAGACA-3′	83–148
	5′-GCCCAATACGACCAAATCC-3′	
GNB2L	5′-GCTACTACCCCGCAGTTCC-3′	170–241
	5′-CAGTTTCCACATGATGATGGTC-3′	
MMP2	5′-ATAACCTGGATGCCGTCGT-3′	2148–2210
	5′-AGGCACCCTTGAAGAAGTAGC-3′	
PAI1	5′-AAGGCACCTCTGAGAACTTCA-3′	53–113
	5′-CCCAGGACTAGGCAGGTG-3′	
CTGF	5′-CTCCTGCAGGCTAGAGAAGC-3′	884–977
	5′-GATGCACTTTTTGCCCTTCTT-3′	
COL1A1	5′-GGGATTCCCTGGACCTAAAG-3′	1869–1928
	5′-GGAACACCTCGCTCTCCA-3′	
SPARC	5′-GTGCAGAGGAAACCGAAGAG-3′	376–439
	5′-TGTTTGCAGTGGTGGTTCTG-3′	
TGM2	5′-GGCACCAAGTACCTGCTCA-3′	1673–1742
	5′-AGAGGATGCAAAGAGGAACG-3′	
TPM1	5′-TGGATCAGACCTTGAAAGCA-3′	790–880
	5′-TCGGAAAGGACCTTGATCTC-3′	
PTGS2	5′-TGGAAGCCTTCTCTAACCTC-3′	512–613
	5′-TCAGGAAGCTGCTTTTTACCTT-3′	
ACTA2	5′-CTGTTCCAGCCATCCTTCAT-3′	1262–1331
	5′-TCAGGAAGCTGCTTTTTACCTT-3′	
TGF-B2	5′-CCAAAGGGTACAATGCCAAC-3′	1194–1283
	5′-CAGATGCTTCTGGATTTATGGTATT-3′	
DCN	5′-ATGCAGCTAGCCTGAAAGGA-3′	1118–1199
	5′-GAGCCATTGTCAACAGCAGA-3′	
BMP4	5′-CTGCAACCGTTCAGAGGTC -3′	225–315
	5′-TGCTCGGGATGGCACTAC-3′	
GREM1	5′-GTGACGGAGCGCAAATACC-3′	406–509
	5′-CCTTCCTCGTGGATGGTCT -3′	